Three-Phase Model for the Reversible Lithiation-Delithiation of SnO Anodes in Li-Ion Batteries

Andreas Pedersen,* Petr A. Khomyakov, and Mathieu Luisier

Integrated Systems Laboratory, Department of Electrical Engineering and Information Technology, ETH Zurich, Gloriastrasse 35, 8092 Zurich, Switzerland

(Received 4 February 2015; revised manuscript received 9 July 2015; published 16 September 2015)

A high reversible capacity is a key feature for any rechargeable battery. In lithium-ion battery technology, tin-oxide anodes do fulfill this requirement, but a fast loss of capacity hinders a full commercialization. Using first-principles calculations, we propose a microscopic model that sheds light on the reversible lithiation-delithiation of SnO and reveals that a sintering of Sn causes a strong degradation of SnO-based anodes. When the initial irreversible transformation ends, active anode grains consist of Li-oxide layers separated by Sn bilayers. During the following reversible lithiation, the Li oxide undergoes two phase transformations that give rise to a Li enrichment of the oxide and the formation of a layered SnLi composite. We find that the model-predicted anode volume expansion and voltage profile agree well with experiments, and a layered anode grain is highly conductive and has a theoretical reversible capacity of 4.5 Li atoms per a SnO host unit. The model suggests that the grain structure has to remain layered to sustain its reversible capacity and a thin-film design of battery anodes could be a remedy for the capacity loss.

DOI: 10.1103/PhysRevApplied.4.034005

I. INTRODUCTION

Tin-based compounds are promising candidates to replace graphite as the anode material in lithium-ion batteries (LIBs) [1]. Having a maximum capacity of 4.4 Li per host atom ($Li_{22}Sn_5$) [2], Sn alloys outperform the theoretical gravimetric limit of graphite by a factor larger than 2 [3]. The interest for Sn-based material systems was originally sparked by the pioneering work of Idota *et al.* [4], who showed that using an amorphous tin composite oxide as the anode of a LIB cell improves the performance of the battery both in terms of capacity and cycleability.

To better understand the behavior of Sn-based materials upon lithiation and delithiation, Courtney and Dahn [5] conducted a series of experiments on various Sn oxides. They found that all the oxides initially undergo an irreversible Li uptake followed by a regime where Li insertion and extraction exhibit a reversible behavior. Using their experimental findings, Courtney and Dahn developed an empirical model where it is assumed that an amorphous Li-oxide matrix forms as the initial Li ions enter the pristine SnO sample. The O atoms are captured by Li, which offers stronger bonds as compared to Sn. At the same time, the Sn atoms are subject to a sintering process and form clusters embedded in the emerging Li-oxide matrix. The proposed Sn clustering model is based on the experimental observation of Sn signatures in x-ray diffraction measurements on the lithiated oxide materials [5]. Note that the aforementioned structural changes of SnO take place during the initial irreversible Li uptake. As the lithiation continues, the Sn clusters are assumed to behave as a $SnLi_x$ alloy, where x is the number of Li atoms per Sn, and should provide a reversible storage medium for Li. The model proposed by Courtney and Dahn has served as a reference for interpreting (de)lithiation of Li-ion battery cells with SnO-based anode electrodes. We adapt this model to Li-O-Sn anodes by assuming that the Sn clusters behave similarly to bulk $SnLi_x$ when exposed to Li. This will be referred to as the *cluster model*.

While the Li-oxide formation and the growth of Sn clusters have been confirmed by many groups [6–10], the actual contribution of these Sn clusters to the reversible lithiation is questionable for several reasons. First, Li oxide is an insulator so that it would be difficult to conceive how electrons can be efficiently supplied to the Sn clusters unless the latter are well interconnected at any stage of lithiation. Second, during the initial phase there exist bond types in the LiOSn sample that cannot be explained by the cluster model [7,8,11,12]. Third, it is well established that the growth of Sn clusters actually causes a capacity degradation of the anode material [10,13,14]. Fourth, the initial stress builds up differently in metallic Sn and insulating SnO during the lithiation process [15] that indicates that the volume expansion profiles are not the same for the two materials. Finally, a recent experiment by Ebner and co-workers [16] has shown that the voltage profile and the volume expansion of SnO oxide during the initial Li insertion-extraction cycle significantly differ from those of a bulk SnLi alloy. Fracturing, which was found to occur at grain boundaries in SnO, is also difficult to explain

*andped10@gmail.com

assuming a homogenous isotropic amorphous Li-oxide matrix and separated Sn clusters.

In this paper, we propose a microscopic model for reversible (de)lithiation of tin monoxide that resolves the shortcomings of the cluster model by Courtney and Dahn [5] summarized in the previous paragraph. Our model is based upon an atomistic study of a large set of structures obtained from first-principles calculations. According to our recent *ab initio* calculations of the irreversible Li uptake of SnO, a fully Li-depleted anode consists of layered Li oxide separated by Sn bilayers [17]. Starting from this configuration, we show here that the Li oxide undergoes two phase transformations as the Li concentration increases, giving rise to the formation of a Li-rich and layered Li oxide (Li_3O). Subsequently, 3.5 additional Li atoms per Sn atom are accommodated solely in Sn layers. Thus, the final structure contains 6.5 Li per Sn atom in total, but the *reversible capacity* of SnO is limited to 4.5 Li per Sn (3.5) and O (1) host atom, whereas the remaining two Li atoms are strongly bound in the Li oxide. By applying this *three-phase model* we are able to reproduce the experimental data for the volume expansion and the voltage profile measured upon lithiation. We also find that the obtained Li-O-Sn model structures exhibit a good in-plane electron conductance because of their highly conductive $SnLi_x$ layers. The results presented here suggest that the undesired degradation of reversible capacity for Li ions might be averted by designing an anode that preserves its layered structure during (de) lithiation. This could be achieved by adopting a thin-film structure on a lattice-matched substrate to promote the layered structure or by inserting species that retard the ongoing Sn sintering process. These general findings could have a wider applicability and be used to better understand the behavior of other metal oxides [18] or Na-ion batteries [19].

II. METHODS

Our first-principles calculations rely on a density-functional plane-wave pseudopotential method within the framework of the generalized gradient approximation [20] and the projector-augmented wave formalism [21], as implemented in the VASP code [22,23]. The equilibrium Li-O-Sn structures consist of a $8 \times 8 \times 1$ SnO supercell (64 Sn and 64 O atoms) with a Li content ranging from 128 to 448 atoms. The supercell Brillouin zone is sampled with a $2 \times 2 \times 2$ k-point grid. The plane-wave kinetic energy cutoff is set at 500 eV. The total energy and forces are converged to at least 10^{-8} eV and 10^{-3} eV/Å, respectively. Further computational details can be found elsewhere [17].

III. THREE-PHASE MODEL

A. Configurations

We now describe in detail the entire process of the anode (de)lithiation as given by the proposed three-phase model. The starting configuration corresponds to the anode grain structure, in which the irreversible uptake of Li is fully complete, and the Li-oxide layers are separated by Sn bilayers as shown in Fig. 1(f). Layers or half layers of Li are inserted into the structure as long as the relative binding energy for Li remains negative

$$E_b = \frac{E_L - (E_{L-1} + N_L E_{\mathrm{Li}})}{N_L}, \tag{1}$$

where E_b is the average relative binding energy of a single Li atom; E_L is the total energy of the anode structure with

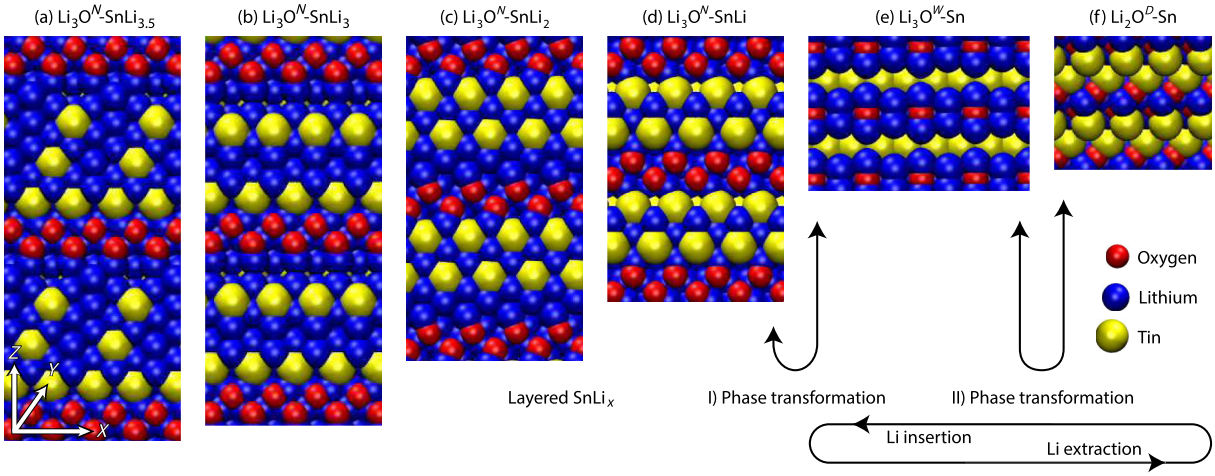

FIG. 1. Reversible lithiation of SnO. Delithiation is from left depicted by the lowermost arrow. Li_yO-$SnLi_x$ structural configurations for x (y) decreasing from 3.5 to 0 (from 3 to 2) and undergoing two phase transformations. The blue, red, and yellow spheres correspond to the Li, O, and Sn atoms, respectively. Initially, 2.5 Li layers are released, causing a Li depletion of $SnLi_x$ from $x = 3.5$ to 1, as shown in insets (a)–(d). The remaining Li layer in the SnLi composite layer is freed as the Li oxide changes its phase from Li_3O^N to Li_3O^W, inset (e). Another phase transformation occurs upon further Li extraction, bringing the Li-rich oxide to its irreversible Li_2O^D phase, inset (f).

L layers of Li; E_{Li} is the cohesive energy of a Li atom in a bulk environment; and N_L is the number of Li atoms in a single Li layer. Structures fulfilling the requirement $E_b < 0$ in Eq. (1) have been determined for Li concentrations up to $L = 6.5$. This Li content corresponds to a fully lithiated SnO sample. For $L \geq 7$ the additional Li atoms are located in the Li-O-Sn structure within an environment similar to bulk Li and have a comparable binding energy so that $E_b > 0$. This indicates that eventual overcharging will result in the formation of domains with bulk Li, which, in the best-case scenario, just act as passive spectators. In other words, having any extra Li atoms in the fully loaded anode structure does not increase the battery capacity since these Li atoms will not be released by the layered anode upon normal discharging conditions.

Figure 1 shows all the structural configurations obtained during the (de)lithiation process described above. As the Li load increases, three different phases can be identified, which are separated by two phase transformations of the Li oxide. The first phase, Li_2O^D, corresponds to the fully Li-depleted configuration in Fig. 1(f). The label D refers to it being a *depleted* structure in which the metallic Sn bilayers surround the insulating Li-poor oxide layers. A second phase, Li_3O^W, as shown in Fig. 1(e), appears upon insertion of the first reversible Li layer. The XY cross section of this oxide layer expands so that the label W stands for its *wider* cross-section area. Note that no substantial change of the supercell size occurs in the Z direction though the Sn bilayer transforms into a monolayer structure. Four structural configurations of a third Li-oxide phase, Li_3O^N, are shown in Figs. 1(a)–1(d). This oxide results from a phase transformation where the number of Li atoms remains unchanged and the Li-rich oxide regains a narrow XY cross section. The label N refers to its *narrower* cross-section area. Hereafter, the inserted Li atoms form a $SnLi_x$ layered composite structure that is accompanied by a strong expansion of the corresponding supercell in the Z direction. The layered composite can accommodate a maximum of 3.5 Li per Sn atom. The fully loaded structural configuration is given in Fig. 1(a). From Fig. 1 it is also apparent that the three-phase model offers an explanation for the "unusual" bond types through a high ratio of both Sn-Sn, Sn-Li, Sn-O, and Li-O bonds in the layered anode grains.

B. Volume expansion

In the present study, we focus only on the first reversible (de)lithiation cycle under the assumption that the initial and irreversible transformation from Sn oxide to Li oxide has already taken place. To validate the three-phase model against the experimental data in Ref. [16], we computed the volume expansion of the Li_yO-$SnLi_x$ anode with respect to the volume of pristine SnO upon Li extraction, as reported in Fig. 2. The volume expansion is defined as

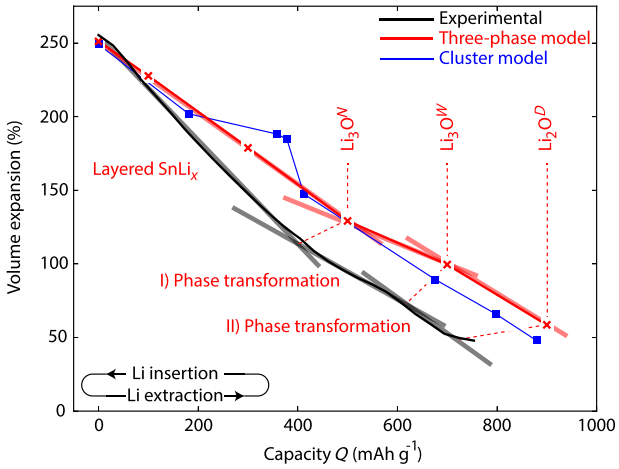

FIG. 2. Volume expansion as a function of Li content for Li-O-Sn anode. The volume expansion is defined with respect to the volume of pristine SnO. Red crosses and filled blue squares refer to the numerical data computed with the three-phase model and the cluster model, respectively. The black, blue, and red solid lines correspond to the experimental data [16], the cluster, and the proposed three-phase model, respectively. The solid lines serve only as a guide to the eye. Three volume expansion regimes can be identified. They are delimited by the three gray straight lines. The delithiation process evolves as follows: (i) Li is released from the $SnLi_x$ composite structure sandwiched between Li_3O^N layers, (ii) the Li oxide transforms into Li_3O^W separated by Sn monolayers, and (iii) a second transformation into the depleted and layered Li_2O^D oxide with Sn bilayers in between occurs.

$$\Delta V = \frac{V - V_{\mathrm{SnO}}}{V_{\mathrm{SnO}}} 100\%, \tag{2}$$

where V is the volume of the Li_yO-$SnLi_x$ supercell at a given Li concentration (x and y), and V_{SnO} is the volume of a pristine SnO structure with the same number of Sn atoms as in the corresponding Li-O-Sn supercell.

The three volume expansion regimes, which can be clearly identified in Fig. 2, correspond to the three Li-oxide phases shown in Fig. 1. At first, Li atoms are released from the $SnLi_x$ composite structure, which is situated in between Li_3O^N layers. This causes a constant volume reduction imposed by the supercell contraction in the Z direction, perpendicular to the XY cross section. While $SnLi_x$ becomes fully Li depleted, the Li-rich oxide undergoes a phase transformation ($N \rightarrow W$) that slows down the volume reduction. Though the atom rearrangement in the anode grain structure is rather drastic, the corresponding volume reduction is quite moderate because of the significant XY cross-section expansion, which compensates for the supercell contraction in the Z direction. Finally, further delithiation extracts the remaining Li atoms that are loosely bound in the oxide, giving rise to another transformation ($W \rightarrow L$). This brings back the anode structure into its depleted state Li_2O^D with a narrow cross section, as depicted in Fig. 1(f). This final transformation induces a strong volume reduction. Figure 2 shows that the volume

expansion, as predicted by the three-phase model, is in a good agreement with the volume change measured in Ref. [16]. We notice that there exists a strong dependence of the anode grain volume on the Li concentration. It may give rise to a deterioration of the layered structure during operation if the Li concentration is inhomogeneous over the anode volume. This could explain why Li oxide has been classified as amorphous in Li-O-Sn anodes [5]. It also explains why fracturing tends to occur at grain boundaries. These fractures take place to relieve accumulated strain in the regions where crystal grains of different orientation and shape intersect during volume expansion and contraction.

C. Voltage profile

To further validate the three-phase model, we calculated the voltage profile of the Li-O-Sn anode during (de) lithiation, as shown in Fig. 3. A previous work on bulk SnLi alloys [24] demonstrated that the voltage profile, which is determined by the change of the Gibbs free energy, can be obtained from the internal energy change only, while the entropy and volume terms can be safely neglected. We adopted a similar approach to compute the voltage profile during delithiation

$$\Delta U = \frac{(E_{\Gamma-\gamma} + \gamma N_L E_{\mathrm{Li}}) - E_\Gamma}{\gamma N_L |e|}, \tag{3}$$

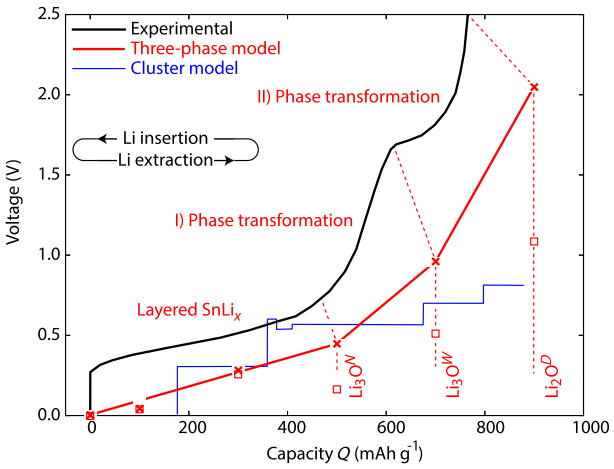

FIG. 3. Voltage profile as a function of Li content for the Li-O-Sn anode. The same plotting conventions as in Fig. 2 are used. Crosses represent voltage with respect to a Li counter electrode and a fully lithiated structure [$\Gamma = 6.5$ and γ varies from 0.5 to 4.5 in Eq. (3)], whereas open boxes correspond to the voltage difference for each lithiation step (Γ varies from 6 to 2 and $\gamma = 1$ except for the first step where $\gamma = 0.5$). The data points for a bulk $SnLi_x$ alloy are shifted along the X axis to coincide with the corresponding points in Fig. 2. The first steplike segment of the voltage profile refers to the $SnLi_x$ delithiation. The two segments with a steeper slope correlate with a phase transformation and a Li depletion of the Li oxide, first from Li_3O^N to Li_3O^W, followed by the phase transformation to Li_2O^D.

where ΔU is the voltage change relative to a reference anode structure with energy E_Γ containing Γ Li layers; $E_{\Gamma-\gamma}$ is the total energy of the anode structure with γ Li layers removed; N_L is the number of Li atoms in a single Li layer, and e is the elementary charge of an electron.

Figure 3 represents the case where the reference is the fully lithiated structure $\Gamma = 6.5$ and shows that a rather moderate increase of the voltage takes place as the Li atoms are released from the $SnLi_x$ composite structure during the first stage of delithiation ($0 < Q < 500$ mAh g^{-1}). A steep voltage increase then occurs as the SnLi composite is depleted of Li atoms and the Li-rich oxide undergoes a phase transformation ($500 < Q < 700$ mAh g^{-1}). Finally, the further extraction of Li atoms from the Li-rich oxide ($700 < Q < 900$ mAh g^{-1}) increases the voltage up to its maximum value of 2.05 eV for the fully Li-depleted anode structure [Fig. 1(f)]. From this it appears that the three-phase model reproduces the experimentally observed voltage profile in a semiquantitative manner [5–7,16]. Figure 3 also shows that the behavior of a bulk SnLi alloy and lithiated SnO oxide is qualitatively different, which demonstrates that the Sn cluster model is not applicable for the Li-O-Sn anode grain.

We notice that the voltage profile given by the three-phase model misses the onset of 0.3 V that is present in the experimental data at the capacity $Q = 0$. This can be explained by the fact that the computed voltage is determined from an average change in the total energy of the anode, as given in Eq. (3), whereas eventual activation energy barriers of the Li atom diffusion process upon delithiation are not accounted for. As a first approximation, the onset voltage can be estimated in the following way. When removing a single Li atom from the anode structure, it appears that the Li atoms residing at the interface between the Li oxide and the composite layers have the weakest bonds. This holds true for all the structures, except the one with a fully-Li-loaded anode [Fig. 1(f)] in which the least bound Li is in the SnLi composite layer. The energy required to extract this Li atom from the composite-layered structure is 0.16 eV, i.e., 0.16 V can be considered as the lower bound for the onset voltage (V_o) at the capacity $Q = 0$.

D. Electron conductance

The anode grain structures, which are given by the three-phase model, are assumed to be good electrical conductors during the entire (de)lithiation cycle. This means that all the layered structures in Figs. 1(a)–1(f) should have a high electron conductance in the XY plane being comparable to that of bulk β-Sn and Li. To confirm this hypothesis, we calculate the band structure of the Li-oxide and SnLi composite layers, which reveals that the oxide layer is an insulator with a sizable band gap that hinders electron transport in the Z direction, whereas the SnLi composite layer is metallic and provides conducting channels for in-plane electron transport. First-principles calculations of

the ballistic electron transport through the SnLi composite layers in Fig. 1 explicitly show that the in-plane electron conductance is comparable to that of bulk β-Sn and Li calculated using the same approach. Hence, the proposed anode structure is a good conductor, which is consistent with experimental observations. Details about the conductance calculations will be published elsewhere [25].

IV. CONCLUSIONS

We have done first-principles, density-functional-theory calculations to understand the reversible lithiation-delithiation of SnO anodes in Li-ion batteries at the microscopic level. Based on these atomistic simulations, we developed a three-phase model that consistently explains how the structural and electronic properties of a SnO-based anode (phase transformation, volume expansion, voltage profile, and electron conductance) evolve during the initial (de)lithiation cycle. This model predicts that the reversible capacity of the SnO-based Li-ion battery can reach up to 4.5 Li atoms per SnO host unit, which is slightly higher than the theoretical capacity for bulk Sn [2]. It also sheds light onto the surprising experimental observation of "unusual" bonds that have been explained by a high ratio of Sn-Sn, Sn-Li, Sn-O, and Li-O bonds in the layered Li-O-Sn structure. Using the obtained results, we proposed a plausible explanation for the deterioration and amorphization of the Li-O-Sn structure, which are attributed to spacial inhomogeneities of the Li concentration in real samples. Finally, the observed capacity degradation of SnO anodes can be understood by applying the cluster model by Courtney and Dahn [5] to describe the slower but irreversible structural changes. A loss in Li capacity results from the system transformation towards its thermodynamically more stable configuration with Sn clusters embedded in a lithium oxide rather than remaining layered as required by the reversible three-phase model.

Our findings suggest that improved SnO-based anodes can be achieved by applying a thin-film design or using an additive to retard the agglomeration of Sn. Furthermore, the layered character of the three-phase model structures appears to be general and might be used to understand the lithiation process of other metal oxides. This is supported by a similarity of voltage profiles measured in Refs. [26,27] for the lithiation of transition metal oxides. The model might also shed light onto the charging dynamics of sodium-ion batteries [28,29], where Na ions replace Li ions as the charge carriers.

ACKNOWLEDGMENTS

This research is funded by the EU Commission (the ERC Starting Grant E-MOBILE). The computer simulations are done at the Swiss National Supercomputer Center (Projects No. s579 and No. s591). The authors thank Martin Ebner for helpful discussions.

[1] M. N. Obrovac, L. Christensen, D. B. Le, and J. R. Dahn, Alloy design for lithium-ion battery anodes, J. Electrochem. Soc. **154**, A849 (2007).
[2] B. A. Boukamp, G. C. Lesh, and R. A. Huggins, All-solid lithium electrodes with mixed-conductor matrix, J. Electrochem. Soc. **128**, 725 (1981).
[3] C.-M. Park, J.-H. Kim, H. Kim, and H.-J. Sohn, Li-alloy-based anode materials for Li secondary batteries, Chem. Soc. Rev. **39**, 3115 (2010).
[4] Y. Idota, Tin-based amorphous oxide: A high-capacity lithium-ion-storage material, Science **276**, 1395 (1997).
[5] I. A. Courtney and J. R. Dahn, Electrochemical and *in situ* x-ray diffraction studies of the reaction of lithium with tin oxide composites, J. Electrochem. Soc. **144**, 2045 (1997).
[6] J. Chouvin, J. Olivier-Fourcade, J. C. Jumas, B. Simon, P. H. Biensan, F. Madrigal, J. L. Tirado, and C. P. Vicente, SnO reduction in lithium cells: Study by x-ray absorption, Sn-119 Mössbauer spectroscopy and x-ray diffraction, J. Electroanal. Chem. **494**, 136 (2000).
[7] Y. Wang, J. Sakamoto, S. Kostov, A. N. Mansour, M. L. denBoer, S. G. Greenbaum, C. K. Huang, and S. Surampudi, Structural aspects of electrochemically lithiated SnO: Nuclear magnetic resonance and x-ray absorption studies, J. Power Sources **89**, 232 (2000).
[8] I. Sandu, T. Brousse, D. M. Schleich, and M. Danot, SnO_2 negative electrode for lithium ion cell: *In situ* Mössbauer investigation of chemical changes upon discharge, J. Solid State Chem. **177**, 4332 (2004).
[9] L. Q. Zhang, X. H. Liu, Y.-C. Perng, J. Cho, J. P. Chang, S. X. Mao, Z. Z. Ye, and J. Y. Huang, Direct observation of Sn crystal growth during the lithiation and delithiation processes of SnO_2 nanowires, Micron **43**, 1127 (2012).
[10] G. Jeong, C. Shin, Y.-J. Kim, H. Lee, and H.-J. Sohn, Aggregation behavior of tin in tin oxides reacted with lithium, Electrochim. Acta **92**, 291 (2013).
[11] I. A. Courtney, R. A. Dunlap, and J. R. Dahn, *In-situ* ^{119}Sn Mössbauer effect studies of the reaction of lithium with SnO and SnO:0.25 B_2O_3:0.25 P_2O_5 glass, Electrochim. Acta **45**, 51 (1999).
[12] I. Sandu, T. Brousse, D. M. Schleich, and M. Danot, The chemical changes occurring upon cycling of a SnO_2 negative electrode for lithium ion cell: *In situ* Mössbauer investigation, J. Solid State Chem. **179**, 476 (2006).
[13] I. A. Courtney and J. R. Dahn, Key factors controlling the reversibility of the reaction of lithium with SnO_2 and Sn_2BPO_6 glass, J. Electrochem. Soc. **144**, 2943 (1997).
[14] M. Behm and J. Irvine, Influence of structure and composition upon performance of tin-phosphate-based negative electrodes for lithium batteries, Electrochim. Acta **47**, 1727 (2002).
[15] H. Tavassol, M. W. Cason, R. G. Nuzzo, and A. A. Gewirth, Influence of oxides on the stress evolution and reversibility during SnO_x conversion and Li-Sn alloying reactions, Adv. Energy Mater. **5**, 1400317 (2014).
[16] M. Ebner, F. Marone, M. Stampanoni, and V. Wood, Visualization and quantification of electrochemical and mechanical degradation in Li ion batteries, Science **342**, 716 (2013).

[17] A. Pedersen and M. Luisier, Lithiation of tin oxide: A computational study, ACS Appl. Mater. Interfaces **6**, 22257 (2014).

[18] W.-J. Zhang, A review of the electrochemical performance of alloy anodes for lithium-ion batteries, J. Power Sources **196**, 13 (2011).

[19] S.-W. Kim, D.-H. Seo, X. Ma, G. Ceder, and K. Kang, Electrode materials for rechargeable sodium-ion batteries: Potential alternatives to current lithium-ion batteries, Adv. Energy Mater. **2**, 710 (2012).

[20] J. P. Perdew, K. Burke, and M. Ernzerhof, Generalized Gradient Approximation Made Simple, Phys. Rev. Lett. **77**, 3865 (1996).

[21] P. E. Blöchl, Projector augmented-wave method, Phys. Rev. B **50**, 17953 (1994).

[22] G. Kresse and J. Furthmuller, Efficient iterative schemes for *ab initio* total-energy calculations using a plane-wave basis set, Phys. Rev. B **54**, 11169 (1996).

[23] G. Kresse and J. Furthmuller, Efficiency of *ab-initio* total energy calculations for metals and semiconductors using a plane-wave basis set, Comput. Mater. Sci. **6**, 15 (1996).

[24] I. A. Courtney, J. S. Tse, O. Mao, J. Hafner, and J. R. Dahn, *Ab initio* calculation of the lithium-tin voltage profile, Phys. Rev. B **58**, 15583 (1998).

[25] P. A. Khomyakov, A. Pedersen, and M. Luisier (unpublished).

[26] P. Poizot, S. Laruelle, S. Grugeon, and L. Dupont, Nano-sized transition-metal oxides as negative-electrode materials for lithium-ion batteries, Nature (London) **407**, 496 (2000).

[27] P. Poizot, S. Laruelle, S. Grugeon, and J. M. Tarascon, Rationalization of the low-potential reactivity of 3D-metal-based inorganic compounds toward Li, J. Electrochem. Soc. **149**, A1212 (2002).

[28] D. Su, C. Wang, H. Ahn, and G. Wang, Octahedral tin dioxide nanocrystals as high capacity anode materials for Na-ion batteries, Phys. Chem. Chem. Phys. **15**, 12543 (2013).

[29] M. H. Han, E. Gonzalo, G. Singh, and T. Rojo, A comprehensive review of sodium layered oxides: Powerful cathodes for Na-ion batteries, Energy Environ. Sci. **8**, 81 (2015).